© Universiti Tun Hussein Onn Malaysia Publisher's Office

JAITA

http://publisher.uthm.edu.my/ojs/index.php/jaita

e-ISSN : 2716-7097

Journal of Advanced Industrial Technology and Application

An MRAS Speed Observer Based on dq-axis Power Winding Flux for Sensorless Control of Standalone BDFIGs

Alameen K. Ebraheem[1,3], Elnail Kamal Eldin Idris[2*], Wei Xu, Senior[3], Yi Liu[3], Jianguo Zhu[4]

[1]Faculty of Engineering and Technology,
Nile Valley University, Atbara, 11111, SUDAN

[2]School of Electrical Engineering,
Sudan Technological University, Omdurman, 11111, SUDAN

[3]The State Key Laboratory of Advanced Electromagnetic Engineering and Technology, School of Electrical and Electronic Engineering, Huazhong University of Science and Technology, Wuhan, 430074, CHINA

[4]School of Electrical and Information Engineering,
University of Sydney, Sydney, NSW 2006, AUSTRALIA

*Corresponding Author

DOI: https://doi.org/10.30880/jaita.2022.03.02.005
Received 01 September 2022; Accepted 20 November 2022; Available online 8 December 2022

Abstract: This paper addresses a new mechanical rotor speed observer for sensorless control of standalone Brushless Doubly-Fed Induction Generators (BDFIGs) based on the dq axis power winding flux Model Reference Adaptive System (MRAS) observer. The observer is integrated in the control method for control the terminal frequency and voltage magnitude under various work conditions. The efficiency of the proposed observer and control strategy is proved by overall simulation results and confirmed by experiments. As illustrated without using physical rotor speed sensors, the sensorless control strategy integrating the proposed speed observer can keep effectively the frequency and amplitude of power winding voltage fixed at various rotor speeds and under various conditions of machine parameter and load changes.

Keywords: Brushless Doubly Fed Induction Generators (BDFIGs), Model Reference Adaptive System (MRAS), sensorless speed control, dq axis PW-flux

1. Introduction

In order to the use of brushes and slip ring, the conventional Doubly-Fed Induction Generator (DFIG) face several disadvantages, like large dimensions, minimum reliability, and large cost required for repair. Furthermore, the brushless Doubly-Fed Induction Generator (BDFIG) has absorbed much attention because of its minimum maintenance cost and high reliability design. The Control Winding (CW) and the Power Winding (PW) with various numbers of pole-pairs to hold the straight coupling between them are contained in the same stator of the BDFIG, and the rotor is particularly designed to offer the cross-coupling between CW and PW [1]-[6]. The BDFIG keep all the merits of the conventional DFIG and has been considered an applicable replacement [5] the standalone BDFIG has appeared very good energy saving effectiveness in variable speed constant frequency ship shaft power generation systems. the Power Winding Side Converter (PSC) is used to feed the variable frequency exciting current to the CW, and the Control Winding Side

*Corresponding author: elneelka@hotmail.com

Converter (CSC) sharing the same dc bus as the PSC is linked to the PW to adjust the dc bus voltage and to obtain the bidirectional power flow as shown in fig.1 [6].

The employ of physical speed sensors has a lot of disadvantages in terms of hardness, cost, cabling and repair. Therefore, the sensorless physical speed control is preferred [7]. Many sensorless control strategies based on an MRAS observers for Doubly Fed Induction Machines (DFIMs) have been completely addressed in the literature [8]-[17], the slip frequency is observed based on reactive power- MRAS observer for the standalone DFIG in [8]. A sensorless control method for DFIG in [9] is proposed based MRAS observer using a stator flux.

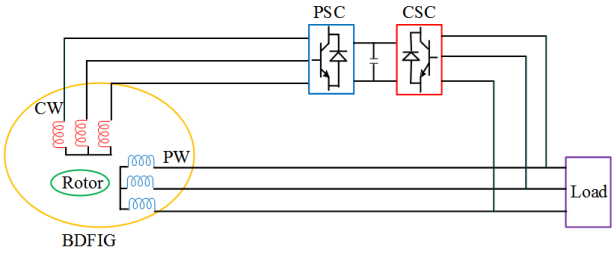

Fig. 1 - Block diagram of BDFIG

The study in [10] presents an MRAS observer for the sensorless control of DFIMs based on the torque and flux rotor current components in the stator-flux oriented axis. A new sensorless control strategy of DFIG based on the MRAS observer using a rotor current has been presented in [11]. A new sensorless rotor position based on electromagnetic torque MRAS observer for DFIG is addressed in [12]. A new control method for sensorless VC of DFIMs based on a rotor current MRAS observer has been proposed in [13]. A sensorless control strategy for grid-connected DFIG based on a back-electromotive force MRAS observer is presented in [14]. A sensorless control method for DFIMs in [15] has been presented for the adjust tuning of the stator inductance in MRAS-rotor current. In [16], a new MRAS for VC of DFIM drive under stator flux orientation has been presented based on a fictitious quantity (ohm). Various MRAS observers are analyzed for the VC method DFIM of stand-alone and connected - grid, using a rotor flux, stator current, stator flux and rotor current in [17].

Only three literatures have address with MRAS for BDFIMs on this topic have been addressed in [18],[19] and [20]. The first difference of the four methods, [18], [19],[20] and the proposed MRAS in this paper, lies in the control aim. The control aims of [19] and the proposed in this paper are the same including the DVC of standalone BDFIG systems in terms of the frequency and voltage amplitude without any physical speed sensors, whereas the control aim of [18] and [20] is the sensorless speed control of BDFIG connected – grid and sensorless speed control of BDFIM respectively. The second difference among the four strategies is the principle of application. Strategy in [18] and [19] use the PW flux as the control component, with integrators to obtain the calculated flux in its stationary reference frame. In [20], the CW current is estimated in the stationary reference frame and employ as the control component. In the proposed Strategy in this paper, the dq axis PW flux is respected as the control component, without the need of the integrator to achieve the calculated flux, based on the rotatory reference frame. Finally, the number of integrators in the physical speed observer employed in [18], [19], [20],[21] and the proposed method in this paper are four, four, four, and two, respectively.

Based on the analysis above, the strategy proposed in this manuscript can be considered as the most distinguished one among the four strategies due to the use of the fewest number of integrators and the consequent lowest complexity in the calculation's operation.

In this paper, the PW-flux MRAS based voltage-oriented control strategy is used to obtain the sensorless control of standalone BDFIG systems. The proposed strategy contains two models, the reference model and the adaptive model using the PW flux.

The paper is regulated as follows. The mathematical model of BDFIG is represented in Section II. The complete design of the proposed MRAS observer is addressed in Section III. Section IV addresses the proposed sensorless control system based on the dq axis PW-flux MRAS observer. The proposed method is simulated in Section V, and verified by experiments in Section VI. Finally, the conclusions are sketched in Section VII.

Nomenclature is included if necessary

$\omega 1, \omega 2$	Angular frequencies of power and control windings (electrical rad/s)
$\tilde{\omega}_r$, ω_r	Estimated and actual rotor angular speeds (mechanical rad/s)
p1, p2	Pole pairs of power and control windings
u, i, ψ	Voltage (V), current (A), and flux linkage (Wb)
U	RMS value of voltage (V)
R_r, R_1, R_2	Resistances of the rotor, power and control windings (Ω)
L_r, L_1, L_2	Self-inductances of the rotor, power and control windings (H)

L_{1r}, L_{2r}	Mutual inductances between the rotor and power windings, and the rotor and control windings (H)
$\tilde{\theta}_r$	Estimated rotor positions (mechanical rad)
S	Differential operator

2. Mathematical Model

In the doubly fed mode, the rotor speed of BDFIG can be expressed as [21]

$$\omega_r = \frac{\omega_1 + \omega_2}{p_1 + p_2} \tag{1}$$

The mathematical vector model of BDFIG in the dq synchronous frame can be derived as [21]

$$u_1 = R_1 i_1 + \frac{d\psi_1}{dt} + j\omega_1 \psi_1 \tag{2}$$

$$0 = R_r i_r + \frac{d\psi_r}{dt} + j(\omega_1 - p_1\omega_r)\psi_r \tag{3}$$

$$u_2 = R_2 i_2 + \frac{d\psi_2}{dt} + j(\omega_1 - (p_1 + p_2)\omega_r)\psi_2 \tag{4}$$

$$\psi_1 = L_1 i_1 + L_{1r} i_r \tag{5}$$

$$\psi_r = L_r i_r + L_{2r} i_2 + L_{1r} i_1 \tag{6}$$

$$\psi_2 = L_2 i_2 + L_{2r} i_r \tag{7}$$

3. MRAS Observer Structure

The proposed MRAS observer, as shown in Fig. 2, has two models, the reference and the adaptive model. The measured stator PW flux obtained from the voltages and currents of the PW is compared to the flux obtained from the PW and CW stator currents. The error is controlled to be equal to zero using a PI controller and the output of this controller is used as the estimation of the rotor speed. Then, this estimated speed is fed back to adjust the adaptive model.

From (2) at steady state, a reference model design can be obtained as

$$\begin{cases} \psi_{1d} = \dfrac{u_{1q} - R_1 i_{1q}}{\omega_1} \\ \psi_{1q} = -\dfrac{u_{1d} - R_1 i_{1d}}{\omega_1} \end{cases} \tag{8}$$

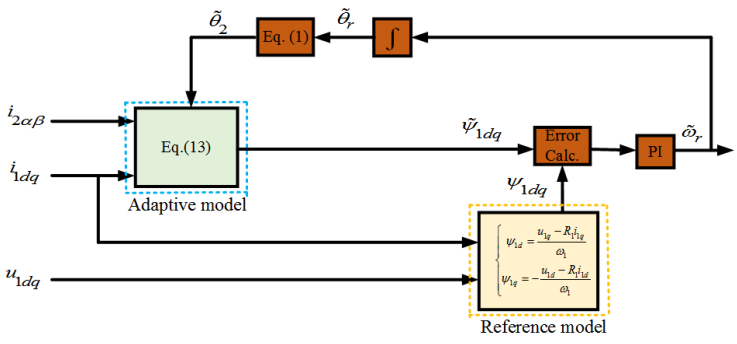

Fig. 2 - Structure of the dq PW-flux MRAS observer

Substituting (6) to (3) yield

$$i_r = \frac{-[s + j(\omega_1 - p_1\omega_r)](L_{2r}i_2 + L_{1r}i_1)}{R_r + [s + j(\omega_1 - p_1\omega_r)]L_r} \quad (9)$$

From equation (5)

$$i_1 = \frac{1}{L_1}\psi_1 - \frac{L_{1r}}{L_1}i_r \quad (10)$$

Substituting (10) to (9), and can be neglected, the rotor current can be obtained as follow:

$$i_r = \frac{(L_1L_{2r}i_2 + L_{1r}\psi_1)}{({L_{1r}}^2 - L_1L_r)} \quad (11)$$

Substituting equation (11) from (5), the PW stator flux is

$$\psi_1 = \frac{(L_1L_r - {L_{1r}}^2)i_1 - (L_{1r}L_{2r})i_2}{L_r} \quad (12)$$

The adaptive model of the estimation of the power winding stator flux in dq reference frame is

$$\tilde{\psi}_{1dq} = \frac{(L_1L_r - {L_{1r}}^2)i_{1dq} - (L_{1r}L_{2r})i_{2dq}}{L_r} \quad (13)$$

The speed can be observed as

$$\tilde{\omega}_r = (K_p + \frac{K_i}{S})(\tilde{\psi}_{1d}.\psi_{1q} - \psi_{1d}.\tilde{\psi}_{1q}) \quad (14)$$

4. Proposed Sensorless Control Based On PW-FLUX MRAS Observer

The PW voltage d-axis component, u_{1d} tracks the PW voltage reference U_1^* through the reference amplitude of CW current i_{2d}^*. The PW voltage q-axis component, u1q, can converge to zero by regulating the CW current frequency, $\omega 2^*$, such that the resultant PW voltage vector overlaps the d-axis of the rotating dq frame, i.e. the PW voltage and frequency can well track their reference values.

The frequency and amplitude of the PW voltage are kept constant at the desired voltage and frequency (in this paper, the reference values are set as 311 V and 50 Hz) under variable rotor speed, load and parameters for the standalone BDFIG system. Fig.3 shows the overall proposed control method.

5. Simulation Results

To prove the effectiveness of the proposed control strategy, several of the obtained simulation results are addressed in this section for a BDFIG when the rotor speed varies from 700 rpm to 600 rpm. The effectiveness of the proposed dq axis PW-flux MRAS observer for sensorless DVC when the parameters change is also approved in this section. The parameters of the simulated system are scheduled in table I.

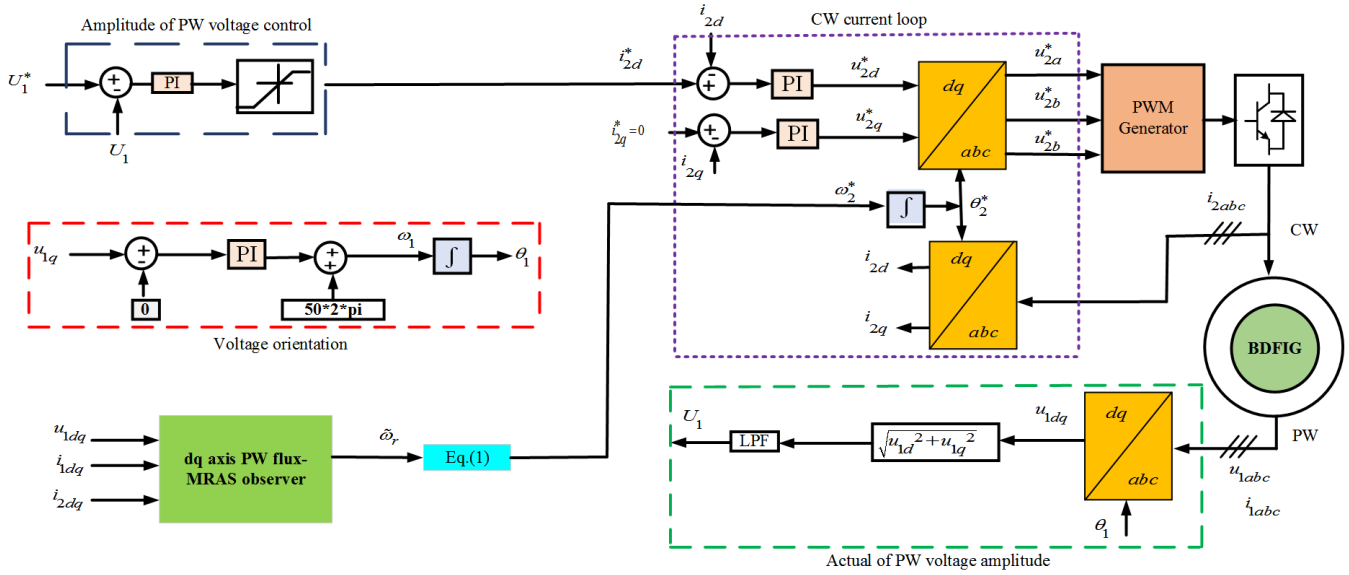

Fig. 3 - Overall block diagram of the proposed sensorless control method for the standalone BDFIG system

Table 1 - Detailed parameters of BDFIG

Parameter	Value
Capacity	30 kVA
Range of speed	600 ~1200 rpm
p_1, p_2	1, 3
PW voltage and current	380 V, 45 A
CW voltage range	0~350 V
CW current range	0~40 A
R_1, R_2, R_r	0.4034 Ω, 0.2680 Ω, 0.3339 Ω
L_1, L_2, L_r	0.4749 H, 0.03216 H, 0.2252 H
L_{1r}, L_{2r}	0.3069 H, 0.02584 H

5.1 Response Under Speed and Load Variation

Fig. 4 illustrates the response when the rotor speed reduces from 700 rpm to 600 rpm at t = 1 s under load vary from 50 Ω to 25 Ω at t=1.2 s for the proposed dq axis PW-flux MRAS observer. Fig. 4 (a)-(g) show the actual and estimated rotor speeds, the detailed actual and estimated rotor speeds, the PW three phase voltages for various periods, and the CW three-phase currents, respectively.

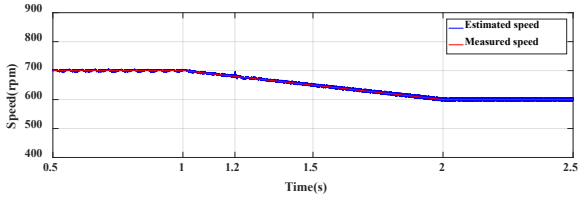

(a)

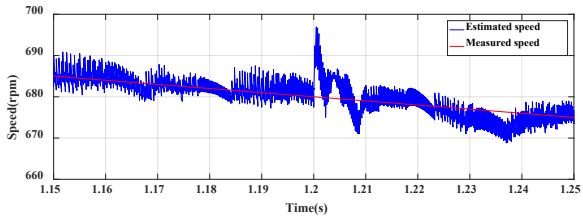

(b)

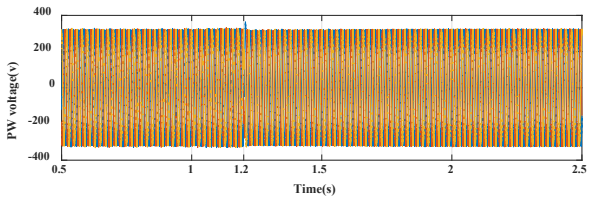

(c)

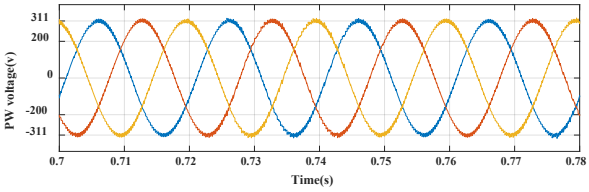

(d)

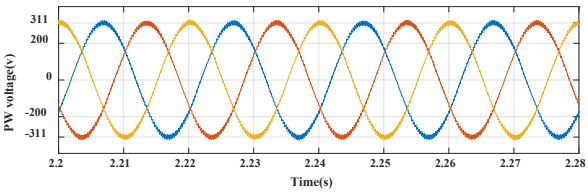

(e)

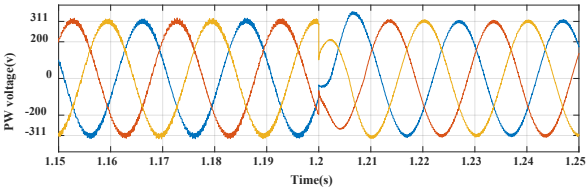

(f)

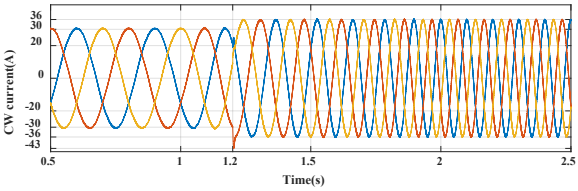

(g)

Fig. 4 - Simulation results under the speed ramp change with load change. (a) actual and estimated rotor speeds. (b) detailed actual and estimated rotor speeds. (c) PW three phase voltages between 0.5 and 2.5 s. (d) PW three phase voltages between 0.7 and 0.78 s (e) PW three phase voltages between 2.2 and 2.28 s. (f) PW three phase voltages between 1.15 and 1.25 s. (g) CW three phase currents

5.2 Effect of Parameters Variations

Figs. 5 and 6 illustrate the response of BDFIG when the parameters change, including the change of PW resistance and the inductances which affect the proposed control method, respectively. The effects were studied with 130% of PW resistance and 150% of the whole inductance values under load change from 25 Ω to 50 Ω at t=1.2 s figs. 5 and 6(a)-(d) show the actual and estimated rotor speeds, the PW three phase voltages for different periods, and the CW three phase currents, respectively.

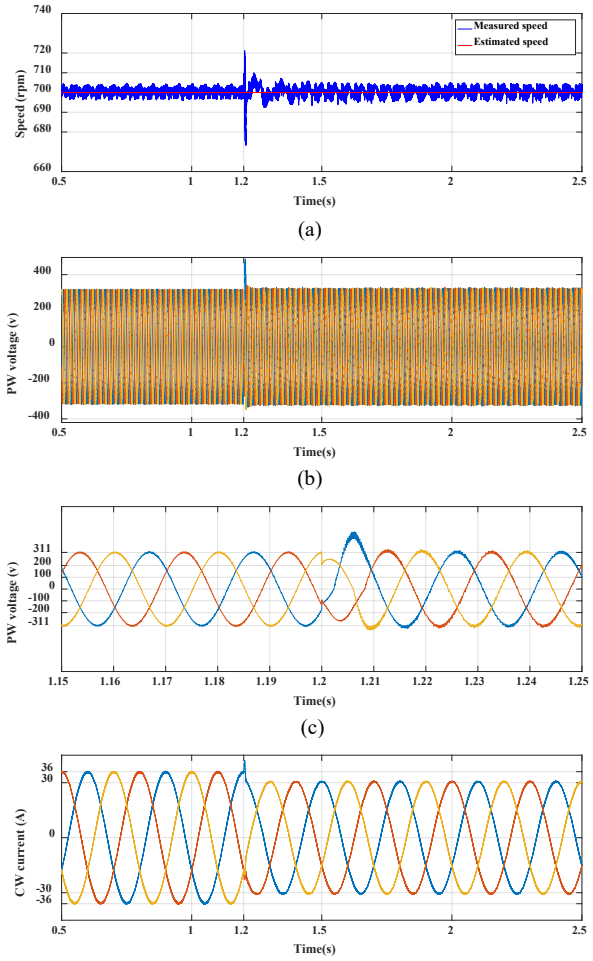

Fig. 5 - Simulation results under 130% variation in PW resistance for the proposed sensorless DVC system of BDFIG. (a) actual and estimated rotor speeds. (b) overall PW three phase voltages. (c) detailed PW three phase voltages between 1.15 and 1.25 s. (c) CW three phase current

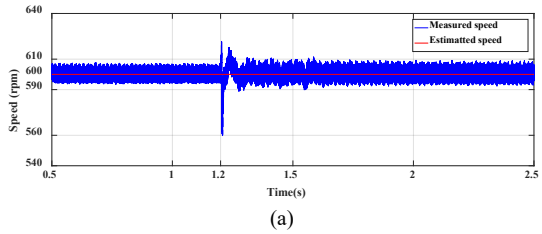

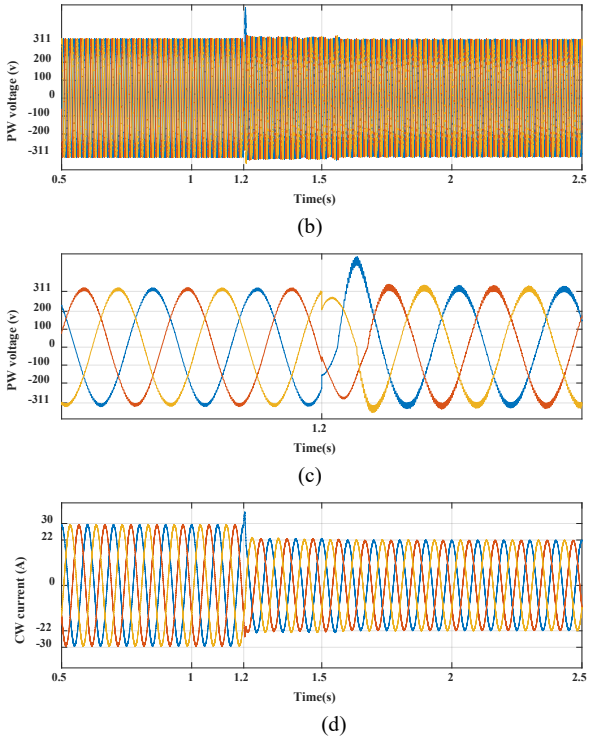

Fig. 6 - Simulation results under 150% variation in the whole inductance. (a) actual and estimated rotor speeds; (b) overall PW three phase voltages; (c) detailed PW three phase voltages between 1.15 and 1.25 s; (d) CW three phase currents

It is noticed from the simulation results, shown in figs. 5 and 6, the proposed sensorless control method is not affected by any variation in the BDFIG parameters including both the PW resistance and the inductances, but they affect the estimation of the generator speed.

The study addressed in this subsection well shows the effectiveness of the proposed sensorless control method based on dq axis PW-flux MRAS observer for DVC of the standalone BDFIG systems with good transient responses. The simulation results prove good tracking implementation for frequency and voltage amplitude control when the rotor speed changes and the load varies. The addressed simulation results verify that the estimated rotor speed is in a good harmony with the measured speed. This ensures the effectiveness of the proposed dq axis PW-flux MRAS observer for the sensorless DVC control system of the standalone BDFIG.

The study addressed in this subsection well shows the effectiveness of the proposed sensorless control method based on dq axis PW-flux MRAS observer for DVC of the standalone BDFIG systems with good transient responses. The simulation results prove good tracking implementation for frequency and voltage amplitude control when the rotor speed changes and the load varies. The addressed simulation results verify that the estimated rotor speed is in a good harmony with the measured speed. This ensures the effectiveness of the proposed dq axis PW-flux MRAS observer for the sensorless DVC control system of the standalone BDFIG.

6. Experimental Results

Overall experiments are achieved to confirm the performance of the proposed sensorless control strategy based on the dq axis PW-flux MRAS observer. Fig. 7 shows the experimental setup of the standalone wound-rotor BDFIG system. This prototype comprises a wound-rotor BDFIG, a prime mover of 37 kW induction motor, a back-to-back converter incorporated with DSP TMS28335 control circuit for linking the PW and the CW and load box. The parameters of the BDFIG system are inducted in table I.

6.1 Constant Load under Variable Speed

The generator speed began from 700 rpm under a three-phase load of 50 Ω per phase, and then is decreased to 600 rpm. Fig. 8(a) shows the estimated speed by the proposed speed observer, which well tracks the actual speed. Fig. 8(b) illustrates the error between the actual and the estimated speed. The control method succeeded in keeping the load voltage fixed at the reference rms value of 150 V as proved in fig. 8(c). The CW current under various speeds is shown in fig. 8(d), and the estimated speed can be confirmed by the frequency of winding current showed in Figs. 8(e) and (f).

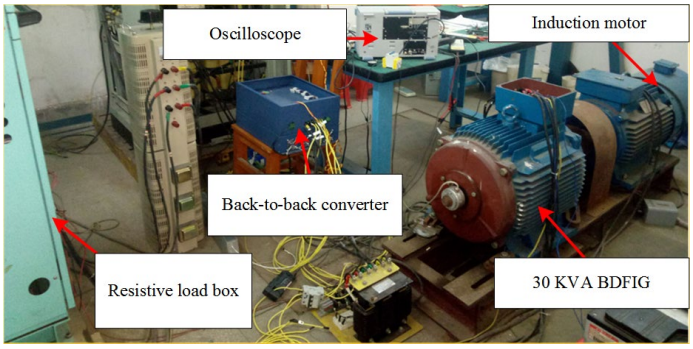

Fig. 7 - Photograph of experimental setup

6.2 Constant Speed Under Variable Load

When the generator speed is fixed at 600 rpm and the load is initially set at 50 Ω per phase and then reduced to 25 Ω per phase, both the actual and estimated speed is shown in fig. 9(a), and the difference between them (error) is showed in fig. 9(b). As illustrated in fig.9(c), the output voltage of the PW is constant at 150 V rms. Fig. 9(d) illustrates the zoomed waveform of the PW voltage to illustrate that the frequency is kept at 50 Hz. The CW current and the zoomed waveform are shown in figs. 9(e) and (f), respectively.

6.3 Variable Load and Variable Speed Under 1.5L Change

The third experiment test is carried out with change speed, change load, and 1.5 increases in all inductances. The generator is initially worked at 700 rpm with a three-phase load of 50 Ω per phase. Then, the speed is decreased to 600 rpm, and during the reduction of the speed, the terminal load is changed from 50 to 25 Ω per phase. As illustrated in fig. 10(a), the estimated speed well tracks the actual speed during the load and speed change. The error is about 0.7% from the reference speed as shown in fig. 10(b). The PW terminal load voltage and the CW current are shown in Figs. 10(c) and (d). The effect of load vary can be observed from the CW current illustrated in Fig. 10(d).

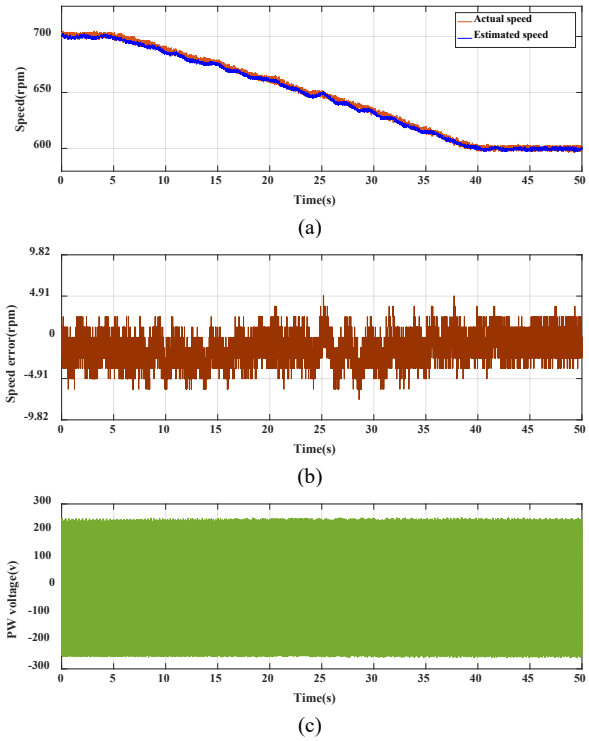

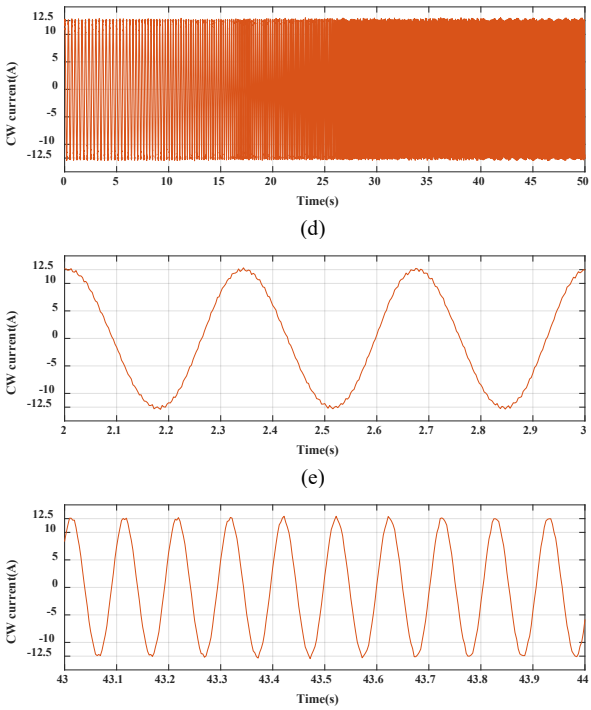

Fig. 8 - Experimental results under variable speed (700 rpm to 600 rpm speed change) for the proposed sensorless DVC system of BDFIG. (a) actual and estimated rotor speed; (b) rotor speed error; (c) PW phase voltage; (d) overall CW phase current; (d) detailed CW phase current between 2 and 3 s; (d) detailed CW phase current between 43 and 44 s

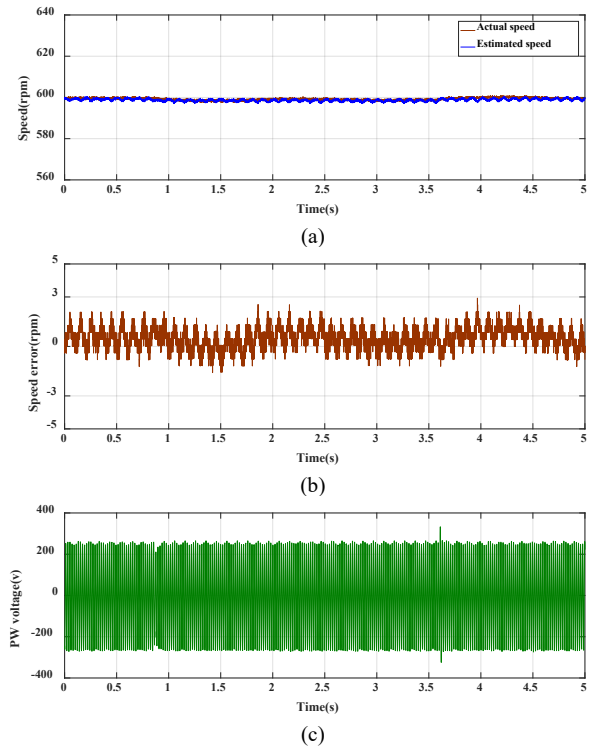

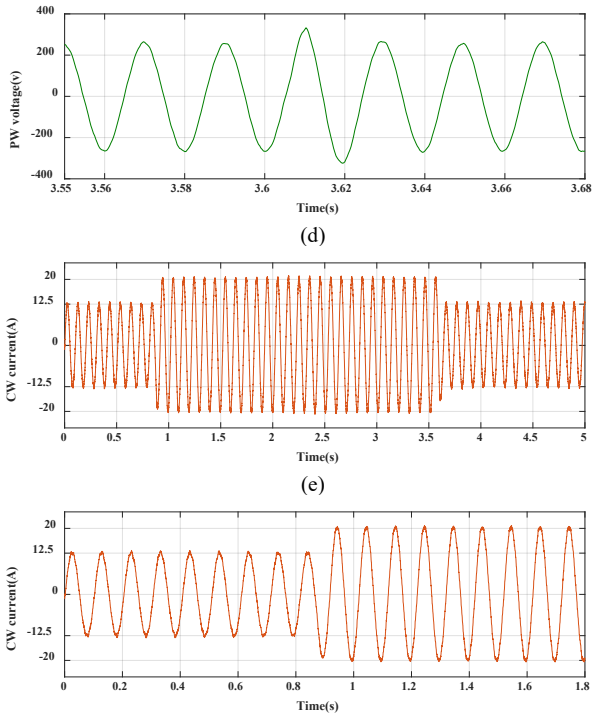

Fig. 9 - Experimental results under variable load with the rotor speed of 600 rpm. (a) actual and estimated rotor speeds; (b) rotor speed error; (c) overall PW phase voltage; (d) detailed PW phase voltage between 3.55 and 3.68 s; (e) overall CW phase current; (f) detailed CW phase current between 0 and 1.8 s

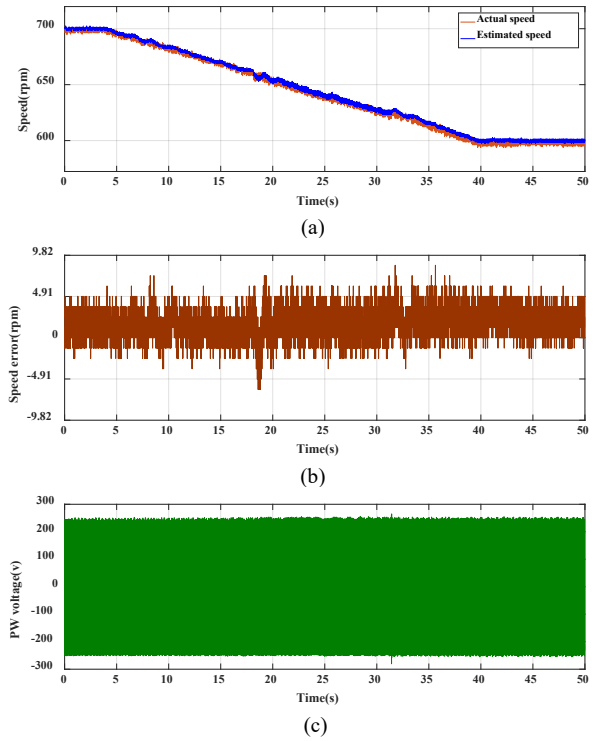

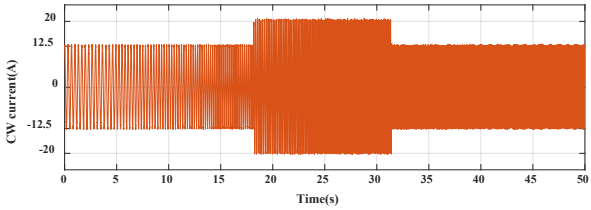

(d)

Fig. 10 - Experimental results under variable speed (700 rpm to 600 rpm speed change and load change under same time) for the proposed sensorless DVC system of BDFIG with 1.5L variation, (a) the actual and estimated rotor speed; (b) rotor speed error; (c) the PW phase voltage; and (d) CW phase current

6.4 Response with Load Change under PW Resistance Variation (1.3 R_1)

To show the effects of parameters changes, e.g. the PW resistance, the fourth experiment test is achieved at a fixed speed with changing load. The generator is firstly operated at 600 rpm with the three-phase load of 50 Ω per phase. At 3.2 s, the terminal load is varied from 50 to 25 Ω per phase as shown in fig. 11. Although the PW circuit resistance varies, the proposed estimation strategy is capable to correctly estimate the actual speed as confirmed by fig. 11(a). The error between the estimate and measured speeds is plotted in fig. 11(b). The maximum value of this error is less than 0.3%from the reference speed. The detailed PW load voltage is illustrated in figs. 11(c) and (d) (zoomed waveform). The effect of load change can be observed from the CW current shown in figs. 11(e) and (f) (zoomed waveform).

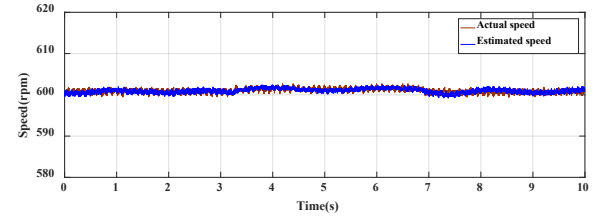

(a)

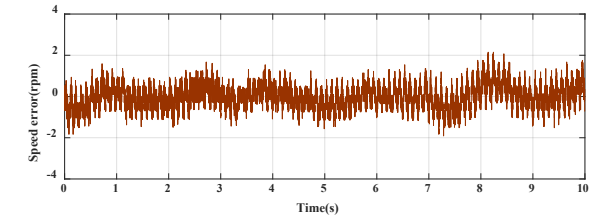

(b)

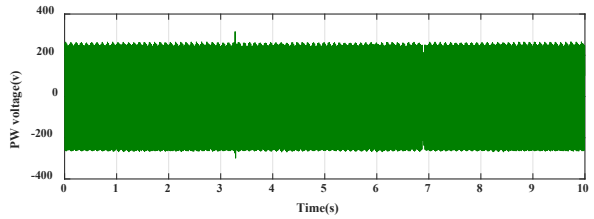

(c)

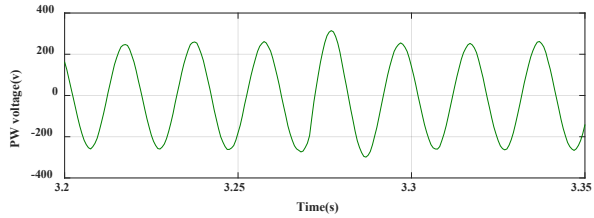

(d)

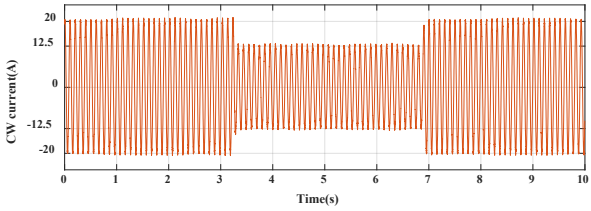

(e)

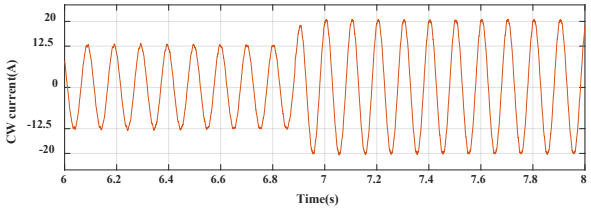

(f)

Fig. 11 - Experimental results under PW resistance variation (1.3 R1) with the speed of 600 rpm. (a) actual and estimated rotor speeds; (b) rotor speed error; (c) overall PW phase voltage; (d) detailed PW phase voltage between 3.2 and 3.35 s; (e) overall CW phase current; (f) detailed CW phase voltage between 6 and 8 s

6.5 Speed Variation and Load Change

To validate the proposed control method, the fifth experiment test is addressed with variable speed from 700 to 600 rpm, under variation load from 50 to 25 Ω per phase. All the experimental results of this case study are schemed in figs. 12(a)-(f), showing the actual and the estimated speeds, the error of speed tracking, the real time and zoomed waveforms of the PW voltage and CW current, respectively. As illustrated by the addressed experimental results, the proposed sensorless control strategy is not affected by any mismatch in the BDFIG parameters, including both the PW resistances and inductances.

Both the simulation and experimental results confirm that the estimated generator speed can track successfully the actual value under different operating conditions, and the proposed sensorless control method based on PW-flux MRAS is effective for standalone BDFIG systems.

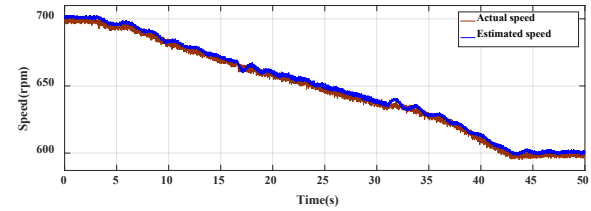

(a)

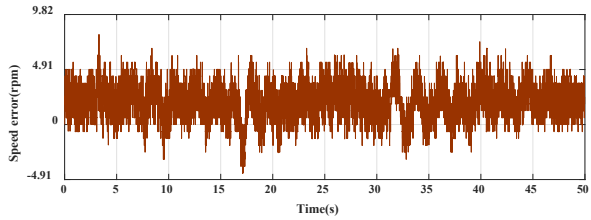

(b)

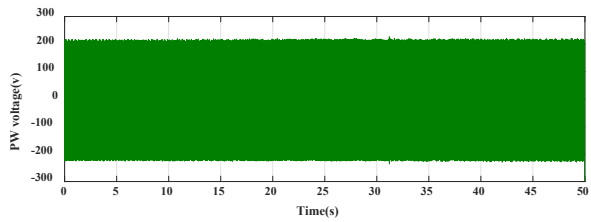

(c)

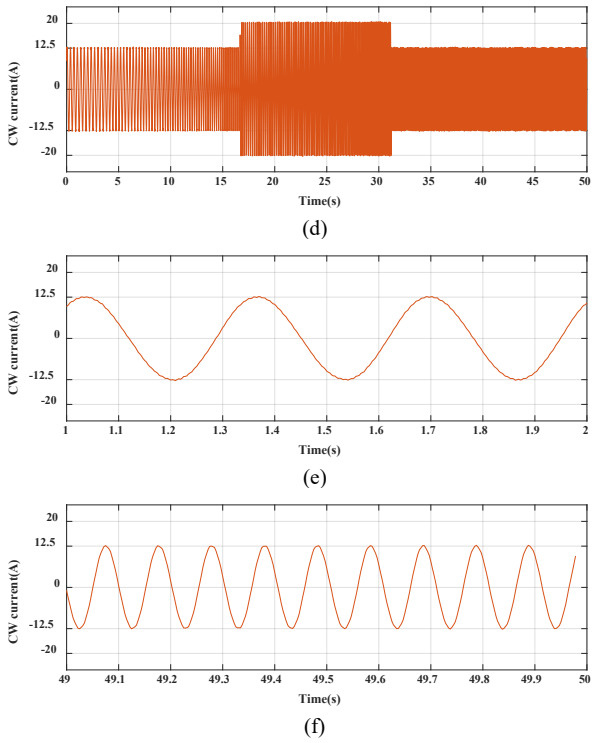

Fig. 12 - Experimental results under (700 rpm to 600 rpm speed change) and load change from 50 to 25 Ω for the proposed sensorless DVC system of BDFIG. (a) actual and estimated rotor speed; (b) rotor speed error; (c) PW phase voltage; (d) overall CW phase current; (e) detailed CW phase current between 1 and 2 s; (f) detailed CW phase current between 49 and 50 s

7. Conclusion

This paper addresses a new MRAS speed observer based on dq PW- flux for sensorless control of standalone BDFIGs. The proposed MRAS observer on dq-PW flux two models, the adaptive model and the reference model. Performance of the addressed control strategy is shown by simulation results and confirmed by experiments. The tested BDFIG has proved good transient behavior under various rotor speeds, load changes and parameter variations under the control of the proposed control strategy based on the dq axis PW-flux MRAS. The results also prove the good tracking between the estimated and actual speed response, proving the strong capability of the proposed sensorless control based on the dq axis PW-flux MRAS observer for standalone BDFIGs.

References

[1] Teng L., Shiyi S., Ehsan A., Richard A. M. & Shi L. (2013). Asymmetrical Low-Voltage Ride Through of Brushless Doubly Fed Induction Generators for the Wind Power Generation. *IEEE Trans. on Energy Convers*., 28(3), pp.502-511.

[2] Lei S., Yu C., Jingyuan S., Debin Zh., Li P. & Yong K. (2018). Decoupling Network Design for Inner Current Loops of Stand-Alone Brushless Doubly Fed Induction Generation Power System. *IEEE Trans. on Power Electron*., 33(2), pp.957-963.

[3] Hamed G., Hashem O. & Ehsan A. (2014). Calculation of Core and Stray Load Losses in Brushless Doubly Fed Induction Generators. *IEEE Trans. on Ind. Electron*., 61(7), pp.3167-3177.

[4] Ramtin S., Seyed M. M., Thomas A. L., Kashkooli M. R. A., Mohammad A. & Sul A. (2019). Voltage-Dip Analysis of Brushless Doubly Fed Induction Generator Using Reduced T-Model. *IEEE Trans. on Ind. Electron*., 66(10), pp.7510-7519.

[5] Ramtin S., Seyed M. M. , Ataei M., Kashkooli M. R. A. & Sul A. (2018). Super-Twisting Sliding Mode Direct Power Control of a Brushless Doubly Fed Induction Generator. *IEEE Trans. on Ind. Electron*, 65(11), pp.9147-9156.

[6] Yi L., Wei X., Teng L. & Frede B. An Improved Rotor Speed Observer for Standalone Brushless Doubly-Fed Induction Generator under Unbalanced and Nonlinear loads. *IEEE Power Electron*. Regular Paper, in press.

[7] Kumar R., Das S. & Manohar M. (2016). Sensorless control of grid-connected doubly-fed induction machine drive using model reference adaptive controller. *IEEE Uttar Pradesh Section International Conference on Electrical, Computer and Electronics Engineering (UPCON* 2016*)*, Varanasi. India. December 9, 2016, pp. 404-409

[8] Cardenas R., Pena R., Proboste J., Asher G. & Clare J. (2004). Rotor current based MRAS observer for doubly-fed induction machines. *Electronic Letters*, 40(12), 1.

[9] Cardenas R., Pena R., Proboste J., Asher G. & Clare J. (2005). MRAS Observer for Sensorless Control of Standalone Doubly Fed Induction Generators. *IEEE Trans. on Energy Convers.,* 20(4), pp. 710-718.

[10] Pena R., Cardenas R., Proboste J., Asher G. & Clare J. (2008). Sensorless control of doubly-fed induction generators using a rotor-current-based MRAS observer. *IEEE Trans. Ind. Electron.*, 55(1), pp. 330-339.

[11] Cardenas R., Pena R., Clare J., Asher G. & Proboste J. (2008). MRAS observers for sensorless control of doubly-fed induction generators. *IEEE Trans. Power Electron.*, 23(3), pp. 1075-1084.

[12] Matteo F. I. (2011). Adaptive Tuning of the Stator Inductance in a Rotor-Current-Based MRAS Observer for Sensorless Doubly Fed Induction-Machine Drives. IEEE Trans. on Industrial Electronics, 58(10), pp. 4683-4692.

[13] Gil D. M. & Duarte M. S. (2012). New Sensorless Rotor Position Estimator of a DFIG Based on Torque Calculations-Stability Study. *IEEE Trans. Energy Convers*., 27(1), pp. 196-203.

[14] Francesco C. D., Gianmaria F., Matteo F. I. & Roberto P. (2012). An MRAS Observer for Sensorless DFIM Drives
With Direct Estimation of the Torque and Flux Rotor Current Components. *IEEE Trans. on Power Electron*, 27, (5), pp.2576-2584.

[15] Pattnaik M. & Kastha D. (2017). Adaptive speed observer for a stand-alone doubly fed induction generator feeding nonlinear and unbalanced loads. *IEEE Trans. Energy Convers*., 27(4), pp. 1018-1026.

[16] Rahul K. & Sukanta D. (2017). MRAS-based speed estimation of grid-connected doubly fed induction machine drive. *IET Power Electron*.,10 (Iss. 7), pp. 726-737.

[17] Lin-Y. L., Nelson F. A., Chia-Chi Ch. & Tzu-Wei Y. (2018). Model Reference Adaptive Back-Electromotive-Force Estimators for Sensorless Control of Grid-Connected DFIGs. *IEEE Trans. on Industry Applications*, 54(2), pp. 1701-1711.

[18] Zhu Y., Zhang X., Liu C. & Chen H. (2012). Study on speed sensorless control of brushless doubly-fed wind power generator based on flux linkage of the power winding. *Proceedings of the 7th International Conference on Power Electronics and Motion Control*, Harbin. China, June 2, 2012, pp. 2453-2456.

[19] Ebraheem A. K., Xu W., Liu Y. & Hussien M. G. (2018). Sensorless direct voltage control based on MRAS observer for the stand-alone brushless doubly-fed induction generator," *Proceedings of the 21st International Conference on Electrical. Machines and Systems (ICEMS 2018)*, Jeju. South Korea. October 7, 2018, pp. 1606-1611.

[20] Yang J., Tang W., Zhang G., Sun Y., Ademi S., Blaabjerg F. & Zhu Q. (2019). Sensorless Control of Brushless Doubly Fed Induction Machine Using a Control Winding Current MRAS Observer. *IEEE Trans. Ind. Electron*., 66(1), pp. 728-738.

[21] Poza J., Oyarbide E., Roye D. & Rodriguez M. (2006). Unified reference frame dq model of the brushless doubly fed machine. *IEE Proc. Electr. Power Appl*., 153(5), pp. 726-734.